Modelling of Non-Stationary Mobile Radio Channels Incorporating the Brownian Mobility Model With Drift

Alireza Borhani and Matthias Pätzold

***Abstract*—This paper is a pioneering attempt to utilize a Brownian motion (BM) process with drift to model the mobile radio channel under non-stationary conditions. It is assumed that the mobile station (MS) starts moving in a semi-random way, but subject to follow a given direction. This moving scenario is modelled by a BM process with drift (BMD). The starting point of the movement is a fixed point in the two-dimensional (2D) propagation area, while its destination is a random point along a predetermined drift. To model the propagation area, we propose a non-centred one-ring scattering model in which the local scatterers are uniformly distributed on a ring that is *not* necessarily centred on the MS. The semi-random movement of the MS results in local angles-of-arrival (AOAs) and local angles-of-motion (AOMs), which are stochastic processes instead of random variables. We present the first-order density of the AOA and AOM processes in closed form. Subsequently, the local power spectral density (PSD) and autocorrelation function (ACF) of the complex channel gain are provided. The analytical results are simulated, illustrated, and physically explained. It turns out that the targeted Brownian path model results in a statistically non-stationary channel model. The interdisciplinary idea of the paper opens a new perspective on the modelling of non-stationary channels under realistic propagation conditions.**

***Index terms* — Channel modelling, Brownian motion, non-stationary channels, local power spectral density, local autocorrelation function.**

I. INTRODUCTION

TO develop mobile communication systems, geometric channel models are recognized as one of the most effective candidates, which allow a highly accurate system performance analysis. As an example, the one-ring scattering model [1]–[3], in which the local scatterers are uniformly distributed on a ring centered on the MS, is an appropriate model capturing the propagation effects in rural and sub-urban propagation areas. The unified disk scattering model (UDSM) [4] is also one of the most general geometric channel models, which covers numerous circularly-symmetric scattering models as special cases, including the one-ring model. In this regard, an overview of the most important geometric channel models can be found in [5].

Geometric channel models often profit from a common simplification, namely the stationarity assumption of the stochastic channel in time. Considering a very short observation time instant justifies a time-invariant AOA at the MS, which then results in a statistically stationary channel model. Many empirical and analytical investigations, e.g., [6]–[8], however, show that this property is only valid for *very* short travelling distances [9]. This calls for the need to develop and analyze stochastic channel models under non-stationary conditions.

Despite the drastic number of investigations on stationary geometric channel models, the literature lacks studies on non-stationary geometric channel models. Only a small number of analytical studies, e.g., [10]–[13], cope with the statistical properties of non-stationary channels. To the best knowledge of the authors, except the non-stationary one-ring scattering model studied in [14], none of the established geometric scattering models listed in [5] has been analyzed under non-stationary conditions. In [14], a non-stationary one-ring channel model has been derived by assuming that the MS moves from the center of the ring to the ring's border on a straight line. In this paper, we further expand the idea of [14] by allowing the MS to randomly fluctuate around a straight line, where its starting point is not necessarily the ring's center. It can be any point inside the ring of scatterers. To this end, we let the MS move in a semi-random way, but subject to follow a given preferred direction. By establishing an analogy between such a motion and the chaotic movement of particles suspended in fluids discovered by Robert Brown (see [15]), we model the travelling path of the MS by a BMD. We coin the term *targeted Brownian path model* to address the proposed path model of the MS. For a given BM process, the randomness of the path can be controlled by a single parameter. By eliminating the randomness of the path, the MS arrives at a fixed destination point via a straight path. Accordingly, the path model of [14] can be obtained as a special case of the proposed targeted Brownian path model.

Moving along a targeted Brownian path results in local AOAs and local AOMs, which are modelled by stochastic processes rather than random variables. We present the first-order density of the AOA and AOM processes in closed form. Expressions for the local PSD of the Doppler frequencies and ACF of the complex channel gain are also provided. Numerical computations at 2.1 GHz illustrate the analytical results and verify the non-stationarity of the channel model. It is shown that non-stationarity in time contradicts the common isotropic propagation assumption on the channel. It is also proved that the one-ring scattering model can be obtained as a special case of the proposed channel model of this paper.

It is worth mentioning that 3D BM processes have been used to model fully random motions of mobile users [16]. However, 1D BM processes with drift have never been used to model semi-random motions of mobile users. Several other mobility models have also been employed in mobile ad hoc networks [17], but not in the area of channel modelling. In a

Manuscript received July 12, 2013; accepted August 1, 2013.

A. Borhani and M. Pätzold are with the Faculty of Engineering and Science, University of Agder, 4898 Grimstad, Norway (e-mails: {alireza.borhani, matthias.paetzold}@uia.no).

ISBN: 978-988-19253-1-2
ISSN: 2078-0958 (Print); ISSN: 2078-0966 (Online)

nutshell, the novelty of this paper arises from the pioneering utilization of the BMD process as a path model for the modelling of non-stationary mobile fading channels.

The remainder of this paper is organized as follows. Section II gives a brief introduction to BM processes as a physical phenomenon, while Section III utilizes the BM process for developing the targeted Brownian path model. Section IV describes the propagation scenario by means of the non-centred one-ring scattering model. The complex channel gain of the proposed channel model is then described in Section V. Section VI investigates the statistical properties of the channel model. Numerical results are provided in Section VII. Finally, Section VIII summarizes our main findings and draws the conclusions.

II. Principles of the BM Process

BM was originally discovered in 1827 by the famous botanist, Robert Brown. It describes the chaotic movement of particles suspended in a fluid or gas [15]. In the 1860s, there were experimentalists who clearly recognized that the motion is due to the impact of suspending molecules. Finally, in 1906, Albert Einstein [18] offered an exact physical explanation of such a motion based on the bombardment of the suspended particles by the atoms of the suspending fluid. In 1908, a mathematical explanation of the BM was provided by Langevin [19][1]. BM processes have a wide range of applications, such as modelling of stock market fluctuations, medical imaging, and fractal theory [21]. In mobile ad hoc networks, 2D BM processes (random walk) are also employed to model irregular motions of mobile nodes [17]. The model is then used for network layer analysis.

A stochastic process $\{B(t) : t \in [0,T]\}$ is said to be a standard BM process if:

1) $B(0) = 0$.
2) $\forall\ 0 \leq s < t \leq T$, the random variable given by the increment $B(t) - B(s)$ follows the Gaussian distribution with zero mean and variance $t - s$, i.e., $B(t) - B(s) \sim N(0, t-s)$.
3) $\forall\ 0 \leq s < t < u < v \leq T$, the increments $B(t) - B(s)$ and $B(v) - B(u)$ are statistically independent.

From the conditions above, it can be concluded that $B(t)$ is a Wiener process with normally and independently distributed increments.

III. Path Modelling

In what follows, we first provide an equivalent spatial representation of the temporal BM process. Subsequently, the proposed local BM process is used to model the targeted motion of the MS along a predetermined drift.

A. Spatial Representation of the BM Process

To establish an analogy between the BM process and the MS movement, let us first assume that the MS starts from a given point with Cartesian coordinates (x_s, y_s) in the 2D plane. The aim is to model the random path starting from (x_s, y_s) via the BM process described in Section II. For this purpose, we establish a mapping from the temporal representation of the BM process $B(t)$ to the spatial representation of the BM process $B(x)$ by replacing the temporal variable t by the spatial variable x. Accordingly, the first condition of the BM process, i.e., $B(0) = 0$, changes to $B(x_s) = 0$. By assuming (x_d, y_d) as the terminal point of the movement, we introduce the scalar standard BM process over the range $[x_s, x_d]$ by means of the spatial stochastic process $B(x)$, which satisfies the following three conditions:

1) $B(x_s) = 0$.
2) $\forall\ x_s \leq x_p < x \leq x_d$, the random variable given by the increment $B(x) - B(x_p)$ follows the Gaussian distribution with zero mean and variance $x - x_p$, i.e., $B(x) - B(x_p) \sim N(0, x - x_p)$.
3) $\forall\ x_s \leq x_p < x < x_q < x_m \leq x_d$, the increments $B(x) - B(x_p)$ and $B(x_m) - B(x_q)$ are statistically independent.

For computational reasons, it is useful to consider the BM process at discrete values of x. To this end, we define $\Delta x = (x_d - x_s)/L$ for some positive integer L. Hence, $B_l = B(x_l)$ denotes the BM process at $x_l = x_s + l\Delta x$ $(l = 0, 1, ..., L)$. Now, with reference to Conditions 2 and 3, it can be concluded that $B_l = B_{l-1} + \Delta B_l$, where each ΔB_l is an independent normal distributed random variable of the form $N(0, \Delta x)$.

B. The Targeted Brownian Path Model

To model the targeted motion of the MS in the 2D plane, we propose a path with a controllable drift in a preferred direction, while the fluctuations of the path are modeled by the spatial BM process B_l. Accordingly, the path $\mathcal{P}$ of the MS is modelled as follows

$$\mathcal{P}: \left\{ (x_l, y_l) \;\middle|\; \begin{array}{l} x_l = x_s + l\Delta x, \\ y_l = a x_l + b + \sigma_y B_l, \end{array} \right\} \tag{1}$$

where $l = 0, 1, ..., L$ is the position index, the variable a denotes the slope of the drift, b is a constant shift along the y-axis, and σ_y allows to control the randomness of the path. Considering the fact that the randomness of the path $\mathcal{P}$ originates inherently from the randomness of the BM process B_l, the parameter σ_y provides an additional degree of freedom to control the randomness. For instance, by setting σ_y to 0, any point on the line represented by $y_l = ax_l + b$ can be reached. Whereas, increasing the value of σ_y reduces the chance of arriving at that point. However, the mean direction of the path remains unchanged. It is also noteworthy that the path model in (1) reduces to that in [14] if $\sigma_y = 0$. The model also enables to incorporate random fluctuations only along a specific line. For instance, by increasing a towards infinity, the fluctuations occur only along the y-axis. The same behaviour can be attained along any other line (axis) if we simply rotate the coordinate system.

In mobile communications, the proposed targeted Brownian path can be a very useful model to describe typical dynamics of users in motion, such as persons walking along a street, but not necessarily along a very smooth path. In vehicular communications, the model can also be used to explain the jittery motion of the vehicle antenna, while the vehicle is moving along a given direction.

IV. The Propagation Scenario

To cope with the scattering effect caused by the propagation area, we propose a non-centred one-ring scattering

[1] A translation of [19] into English has been provided in [20].

ISBN: 978-988-19253-1-2
ISSN: 2078-0958 (Print); ISSN: 2078-0966 (Online)

model, in which the local scatterers are uniformly distributed on a ring that is not necessarily centred on the MS. The displacement of the MS from the ring's center results in a non-isotropic channel model. This model is an appropriate geometric scattering model to explain environments, in which the base station (BS) antenna is highly elevated to scattering-free levels, while the MS antenna is surrounded by a large number of local scatterers. This situation occurs mostly in rural and sub-urban areas.

Fig. 1 shows the proposed non-centred one-ring scattering model with the uniform distribution of the local scatterers S_n $(n = 1, 2, ..., N)$ on a ring of radius R centered on the origin. In this regard, α_n^S denotes the angle-of-scatterer (AOS) associated with the nth scatterer. At a reference point in time t_0, the MS starts its movement from (x_0, y_0) and tracks the path $\mathcal{P}$ to reach (x_L, y_L) at time t_L. The position of the MS at time $t_l \in [t_0, t_L]$ is described by Cartesian coordinates (x_l, y_l). It is also assumed that the MS is moving with a constant velocity v_R in the direction indicated by the AOM $\alpha_v[l]$. Owing to high path loss, we assume that at time t_l, a wave emitted from the BS reaches the MS at the AOA $\boldsymbol{\alpha}_n^R[l]$ after a single bounce by the nth randomly distributed scatterer S_n located on the ring. A realization of the proposed Brownian path $\mathcal{P}$ in such a geometric scattering model is shown in Fig. 2, in which the starting point (x_0, y_0) of the path is set to the ring's center[2].

The above mentioned propagation scenario is completely different from the one-ring scattering model [1]–[3], in which the MS is located at the center of the ring, while its AOM is a deterministic variable. Therein, considering a very short observation time results in a stationary and isotropic channel model, while herein, the proposed path $\mathcal{P}$ justifies a non-stationary non-isotropic channel model. The proposed jittery path model $\mathcal{P}$ is also different from the smooth path model of [14]. Indeed, the random behavior of the AOM $\alpha_v[l]$ (see Fig. 2) allows a much more flexible non-stationary channel model than the one proposed in [14]. In what follows, after providing an expression for the complex channel gain, we study the statistical properties of the proposed non-stationary channel model.

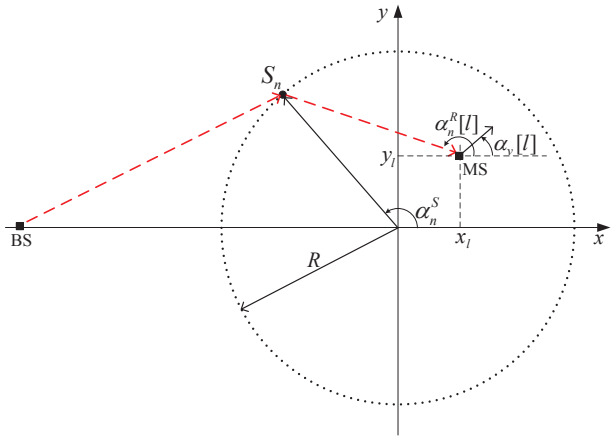

Fig. 1. The non-centred one-ring scattering model for a single-bounce scattering scenario.

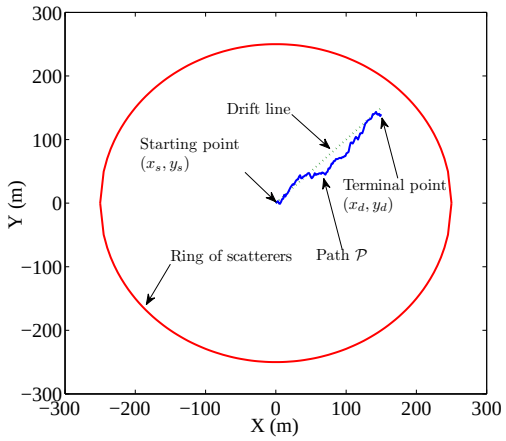

Fig. 2. Realization of a targeted Brownian path $\mathcal{P}$ in the ring of scatterers. The model parameters are $L = 100$, $a = 1$, $b = 0$, $\sigma_y = 2$, $x_s = 0\,\text{m}$, $x_d = 150\,\text{m}$, and $R = 250\,\text{m}$.

V. The Complex Channel Gain

The propagation scenario presented in Section IV is a non-stationary version of the typical fixed-to-mobile (F2M) scenario studied in [22, pp. 56–60]. Therein, the complex channel gain $\boldsymbol{\mu}(t_l)$ of frequency-nonselective F2M channels was modeled by means of a complex stochastic process representing the sum of all scattered components as follows

$$\boldsymbol{\mu}(t_l) = \lim_{N\to\infty} \sum_{n=1}^{N} \boldsymbol{c}_n e^{j(2\pi \boldsymbol{f}_n t_l + \boldsymbol{\theta}_n)}. \tag{2}$$

In the equation above, $\boldsymbol{c}_n$ denotes the attenuation factor caused by the physical interaction of the emitted wave with the nth scatterer S_n, and $\boldsymbol{f}_n$ stands for the Doppler frequency[3] caused by the movement of the MS. In addition, the random variable $\boldsymbol{\theta}_n$ represents the phase shift of the nth path, which is often assumed to be uniformly distributed between 0 and 2π [22, p. 59].

The complex channel gain in (2) suits the proposed non-stationary one-ring model, if we replace the Doppler frequency $\boldsymbol{f}_n$ by $\boldsymbol{f}_n(t_l)$. This apparently minor change adds a great deal of mathematical computations to the statistical characterization of the channel.

VI. Statistical Properties of the Channel

To investigate the statistical properties of the complex channel gain described in (2), let us start from the local AOA, which plays a key role in other statistical quantities. Notice that we defer the illustration and physical explanation of the analytical results to Section VII.

[2]We have chosen the ring's center as the starting point of the movement to enable the verification of our numerical results (see Section VII) with the ones from the one-ring scattering model. However, the analytical results provided in the paper are not limited to such a special case.

[3]The frequency shift caused by the Doppler effect is given by $\boldsymbol{f} = f_{\max}\cos(\boldsymbol{\alpha})$, where $f_{\max} = f_0 v/c_0$ is the maximum Doppler frequency, f_0 denotes the carrier frequency, c_0 stands for the speed of light, and $\boldsymbol{\alpha}$ equals the difference between the AOA and the AOM [23].

ISBN: 978-988-19253-1-2
ISSN: 2078-0958 (Print); ISSN: 2078-0966 (Online)

A. The Local AOAs

Referring to the geometric scattering model in Fig. 1, the AOA $\boldsymbol{\alpha}_n^R[l]$ at the point (x_l, y_l) is given by

$$\boldsymbol{\alpha}_n^R[l] = \arctan\left(\frac{R\sin(\alpha_n^S) - y_l}{R\cos(\alpha_n^S) - x_l}\right). \quad (3)$$

For a given position l, the only random variable in the right side of (3) is the AOS α_n^S. Since the number N of local scatterers tends to infinity in the reference model, it is mathematically convenient to assume that the discrete AOS α_n^S is a continues random variable α^S, which is assumed to be uniformly distributed between $-\pi$ and π (see Section IV). By applying the concept of transformation of random variables [24, p. 130] and performing some mathematical manipulations, it can be shown that the first-order density $p_{\boldsymbol{\alpha}^R}(\alpha^R; l)$ of the stochastic process $\boldsymbol{\alpha}^R[l]$ in (3) becomes

$$p_{\boldsymbol{\alpha}^R}(\alpha^R;l)=\frac{1}{2\pi}\left(1-\frac{x_l\cos(\alpha^R)+y_l\sin(\alpha^R)}{\sqrt{R^2-\left(x_l\sin(\alpha^R)-y_l\cos(\alpha^R)\right)^2}}\right) \quad (4)$$

in which $-\pi \leq \alpha^R < \pi$. It is worth mentioning that $p_{\boldsymbol{\alpha}^R}(\alpha^R; l)$ in (4) depends strongly on the position (x_l, y_l) of the MS. This means that the AOA $\boldsymbol{\alpha}^R[l]$ is *not* first-order stationary. As a special case, if the path $\mathcal{P}$ crosses the ring's center $(0, 0)$, then $p_{\boldsymbol{\alpha}^R}(\alpha^R; l)$ in (4) reduces to $1/(2\pi)$, which is the AOA probability density function (PDF) of the one-ring model [1]–[3].

B. The Local AOMs

By performing the linear interpolation scheme, the path $\mathcal{P}$ becomes continues and piecewise differentiable. This allows us to present the AOM $\boldsymbol{\alpha}_v[l]$ at the location point (x_l, y_l) by the following expression

$$\begin{aligned}\boldsymbol{\alpha}_v[l] &= \arctan\left(\frac{y_{l+1}-y_l}{x_{l+1}-x_l}\right)\\ &= \arctan\left(a+\sigma_y\frac{B_{l+1}-B_l}{x_{l+1}-x_l}\right).\end{aligned} \quad (5)$$

In the right side of (5), $B_{l+1} - B_l$ is the only random variable, which follows the Gaussian distribution of the form $N(0, \Delta x)$ (see Section III-A). Again, by applying the concept of transformation of random variables, the PDF $p_{\boldsymbol{\alpha}_v}(\alpha_v)$ of the AOM $\boldsymbol{\alpha}_v[l]$ in (5) is given by

$$p_{\boldsymbol{\alpha}_v}(\alpha_v) = \frac{1}{\sqrt{2\pi}\sigma\cos^2(\alpha_v)}e^{\frac{-(\tan(\alpha_v)-a)^2}{2\sigma^2}} \quad (6)$$

where $-\pi/2 \leq \alpha_v \leq \pi/2$ and $\sigma = \sigma_y/\sqrt{\Delta x}$. Notice that $p_{\boldsymbol{\alpha}_v}(\alpha_v)$ in (6) is independent of the position (x_l, y_l) of the MS, meaning that the AOM $\boldsymbol{\alpha}_v$ is first-order stationary. It can be shown that the mean $\boldsymbol{\alpha}_v$ equals $\arctan(a)$, in which a is the slope of the drift of the path $\mathcal{P}$.

C. The Local PSD

Considering the local AOA $\boldsymbol{\alpha}^R[l]$ at the MS and the local AOM $\boldsymbol{\alpha}_v[l]$ of the MS, the local frequency shift $\boldsymbol{f}[l]$ caused by the Doppler effect is defined by the following expression

$$\boldsymbol{f}[l] = f_{\max}\cos\left(\boldsymbol{\alpha}^R[l] - \alpha_v[l]\right) \quad (7)$$

in which $\boldsymbol{\alpha}^R[l]$ and $\alpha_v[l]$ are statistically described by the first-order density $p_{\boldsymbol{\alpha}^R}(\alpha^R; l)$ in (4) and the PDF $p_{\boldsymbol{\alpha}_v}(\alpha_v)$ in (6), respectively. The equation above is indeed a non-linear transformation of the stochastic process $\boldsymbol{\alpha}[l] = \boldsymbol{\alpha}^R[l] - \alpha_v[l]$ to the stochastic process $\boldsymbol{f}[l]$. Fixing the position index l and applying again the concept of transformation of random variables results in the first-order density $p_{\boldsymbol{f}}(f; l)$ of the stochastic process $\boldsymbol{f}[l]$ presented in (8) [see the top of the next page], in which $p_{\boldsymbol{\alpha},\boldsymbol{\alpha}_v}(\alpha, \alpha_v; l)$ is given in (9). Notice that the Doppler frequency f in (8) varies between $-f_{\max}$ and $f_{\max}$.

Following the same procedure provided in [22, p. 85], it can be verified that the first-order density $p_{\boldsymbol{f}}(f; l)$ of the Doppler frequencies is directly proportional to the local PSD $S_{\boldsymbol{\mu}\boldsymbol{\mu}}(f; l)$ of the complex channel gain $\boldsymbol{\mu}(t_l)$, i.e.,

$$S_{\boldsymbol{\mu}\boldsymbol{\mu}}(f; l) = 2\sigma_0^2 p_{\boldsymbol{f}}(f; l) \quad (10)$$

where $2\sigma_0^2$ is the mean power of $\boldsymbol{\mu}(t_l)$ and $p_{\boldsymbol{f}}(f; l)$ is provided in (8). If the path $\mathcal{P}$ goes through the ring's center $(0, 0)$, the joint PDF $p_{\boldsymbol{\alpha},\alpha_v}(\alpha, \alpha_v; l)$ in (9) reduces to $p_{\alpha_v}(\alpha_v)/(2\pi)$. Substituting this result in $p_{\boldsymbol{f}}(f; l)$ presented in (8) and then multiplying the answer by the mean power $2\sigma_0^2$, gives the following local PSD

$$S_{\boldsymbol{\mu}\boldsymbol{\mu}}(f; l) = \frac{2\sigma_0^2}{\pi f_{\max}\sqrt{1-(f/f_{\max})^2}}. \quad (11)$$

The equation above represents the PSD of the one-ring scattering model, which is known as the Jakes PSD [23]. Accordingly, the proposed channel model can locally meet the one-ring scattering model.

D. The Local ACF

With reference to the generalized Wigner-Ville spectrum [25, pp. 282-285], the local ACF $r_{\boldsymbol{\mu}\boldsymbol{\mu}}(\tau; l)$ of the non-stationary complex channel gain $\boldsymbol{\mu}(t_l)$ can be attained by taking the inverse Fourier transform of the local PSD $S_{\boldsymbol{\mu}\boldsymbol{\mu}}(f; l)$ in (10). Accordingly, one can write

$$r_{\boldsymbol{\mu}\boldsymbol{\mu}}(\tau; l) = \int_{-f_{\max}}^{f_{\max}} S_{\boldsymbol{\mu}\boldsymbol{\mu}}(f; l)e^{j2\pi f\tau}df. \quad (12)$$

As a special case, if the path $\mathcal{P}$ goes across the ring's center, the local PSD $S_{\boldsymbol{\mu}\boldsymbol{\mu}}(f; l)$ in (11) can be used to compute the inverse Fourier transform in (12). In this case, the local ACF $r_{\boldsymbol{\mu}\boldsymbol{\mu}}(\tau; l)$ in (12) is simplified to $2\sigma_0^2 J_0(2\pi f_{\max}\tau)$, where $J_0(\cdot)$ denotes the zeroth-order Bessel function of the first kind [26, Eq. (8.411.1)].

VII. Numerical Results

Channel modelling at the 2 GHz band is of great importance in mobile communications. With reference to the operating frequency of the universal mobile telecommunications system (UMTS), the carrier frequency $f_0 = 2.1$ GHz has been chosen in our numerical computations. In addition, we consider the path $\mathcal{P}$ shown in Fig. 2 as the travelling path of the MS. This allows us to have the positions (x_l, y_l) for $l = 0, 1, ..., L$. It is also assumed that the MS is moving with a velocity v_R of 80 km/h, which results in a maximum Doppler frequency $f_{\max}$ of 155.5 Hz. The mean power $2\sigma_0^2$ has been set to unity.

ISBN: 978-988-19253-1-2
ISSN: 2078-0958 (Print); ISSN: 2078-0966 (Online)

$$p_{\boldsymbol{f}}(f;l) = \frac{1}{f_{\max}\sqrt{1-(f/f_{\max})^2}} \int_{-\pi/2}^{\pi/2} \Big(p_{\boldsymbol{\alpha},\alpha_v}(\arccos(f/f_{\max}),\alpha_v) + p_{\boldsymbol{\alpha},\alpha_v}(-\arccos(f/f_{\max}),\alpha_v) \Big) d\alpha_v \tag{8}$$

$$p_{\boldsymbol{\alpha},\boldsymbol{\alpha}_v}(\alpha,\alpha_v;l) = \frac{1}{2\pi\sqrt{2\pi}\sigma\cos^2(\alpha_v)} \left| 1 - \frac{x_l\cos(\alpha+\alpha_v)+y_l\sin(\alpha+\alpha_v)}{\sqrt{R^2-(x_l\sin(\alpha+\alpha_v)-y_l\cos(\alpha+\alpha_v))^2}} \right| e^{\frac{-(\tan(\alpha_v)-a)^2}{2\sigma^2}} \tag{9}$$

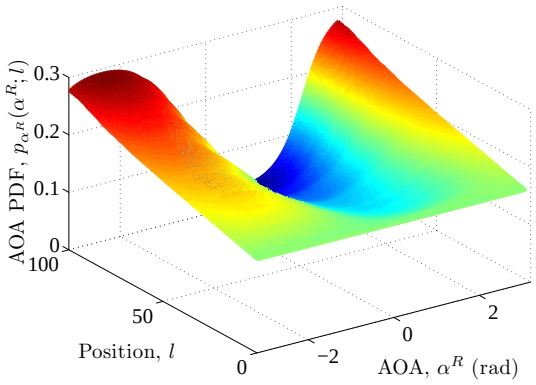

Fig. 3. The behavior of the first-order density $p_{\boldsymbol{\alpha}^R}(\alpha^R;l)$ in (4) for the propagation scenario illustrated in Fig. 2.

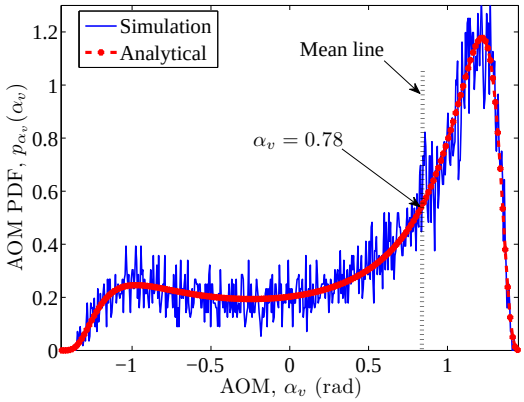

Fig. 4. The behavior of the AOM PDF $p_{\alpha_v}(\alpha_v)$ in (6) for the propagation scenario illustrated in Fig. 2.

Fig. 3 illustrates the first-order density $p_{\boldsymbol{\alpha}^R}(\alpha^R;l)$ of the AOA process $\boldsymbol{\alpha}^R[l]$ provided in (4). With reference to the path $\mathcal{P}$ shown in Fig. 2, the MS starts its movement from the center of the ring. This circularly symmetric starting point explains the uniform distribution of the AOA at $l = 0$. By moving along the path $\mathcal{P}$, the probability of receiving signals from the scatterers ahead reduces, whereas the probability of receiving from the scatterers behind increases. This behavior continuous up to $l = 100$, where $p_{\boldsymbol{\alpha}^R}(\alpha^R,100)$ takes its minimum value at $\alpha^R = \arctan(1) = 0.78$ radian.

Fig. 4 displays the PDF $p_{\alpha_v}(\alpha_v)$ of the AOM $\alpha_v[l]$ in (6). The simulated AOM is also shown in this figure. An excellent match between the simulation and analytical results can be observed. The mean α_v equals $\arctan(1) = 0.78$ radian as shown in the figure. The plot shows explicitly the tendency of the MS to follow the predetermined drift of the path $\mathcal{P}$. This tendency depends solely on the slope a of the drift, which has been set to 1 herein. It is noteworthy that if the randomness σ_y of the path tends to zero, the AOM PDF approaches the delta function at $\alpha_v = 0.78$ radian.

Fig. 5 depicts the local PSD $S_{\boldsymbol{\mu\mu}}(f;l)$ presented in (10). The classical Jakes PSD with a U-shape can be observed in the stationary case ($l = 0$), where the MS is located at the ring's center. At this position, $S_{\boldsymbol{\mu\mu}}(f,0)$ is a symmetric function with respect to f, indicating that the channel is instantaneously isotropic. However, this feature does not hold if the MS continuous its motion along the path $\mathcal{P}$. In this regard, by increasing l, an asymmetric behavior of the local PSD $S_{\boldsymbol{\mu\mu}}(f;l)$ can be observed. Notice that moving along the path $\mathcal{P}$ results in confronting a lower number of scatterers ahead and a higher number of them behind the MS. This allows a higher and a lower probability of negative and positive Doppler shifts as shown in Fig. 5.

Fig. 6 shows the absolute value of the local ACF $r_{\boldsymbol{\mu\mu}}(\tau;l)$ given in (12). Notice that due to the asymmetric behavior of the PSD $S_{\boldsymbol{\mu\mu}}(f;l)$ (see Fig. 5), the ACF $r_{\boldsymbol{\mu\mu}}(\tau;l)$ is in general complex. A quite time-varying behavior of the ACF can be observed. It is also noteworthy that for a given time difference $\tau \neq 0$, the correlation increases through some fluctuations if l grows.

ISBN: 978-988-19253-1-2
ISSN: 2078-0958 (Print); ISSN: 2078-0966 (Online)

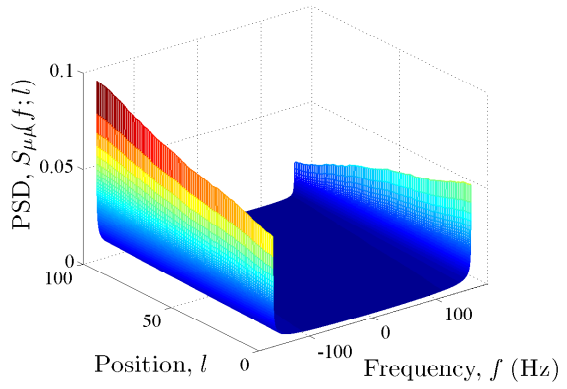

Fig. 5. The behavior of the local PSD $S_{\mu\mu}(f;l)$ in (10) for the propagation scenario illustrated in Fig. 2.

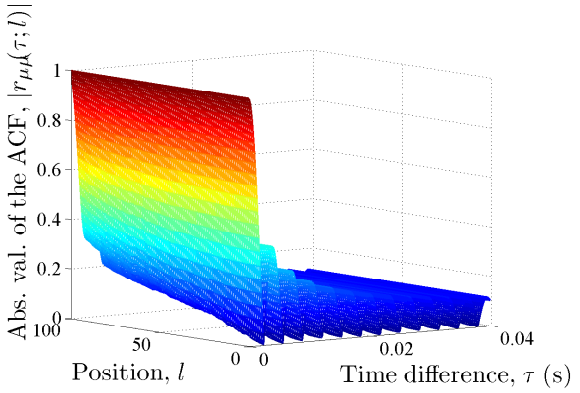

Fig. 6. The behavior of the absolute value of the local ACF $|r_{\mu\mu}(\tau;l)|$ (see (12)) for the propagation scenario illustrated in Fig. 2.

VIII. Conclusion

In this paper, we have proposed a targeted Brownian path model to explain the travelling path of the MS. The proposed path model has a tendency to follow a preferred direction. To describe the propagation area, we have proposed a non-centred one-ring scattering model, in which the MS is not necessarily located at the ring's center. We have assumed that the MS is moving along the proposed targeted Brownian path model in such a geometric scattering model. It has been turned out that the proposed path model results in a non-stationary non-isotropic channel model. As a special case, the stationary isotropic one-ring scattering model can also be obtained from the proposed non-stationary channel model. The statistical properties of the proposed channel model have been derived, illustrated, and discussed extensively. It has been shown that the AOA process is first-order non-stationary, while the PDF of the AOM is stationary. The corresponding PSD of the Doppler frequencies and ACF of the complex channel gain have also been provided, showing that these characteristics are heavily time-dependent. Validating the analytical results by means of empirical data needs to be addressed in future works.

References

[1] D.-S. Shiu, G. J. Foschini, M. J. Gans, and J. M. Kahn, "Fading correlation and its effect on the capacity of multielement antenna systems," *IEEE Trans. Commun.*, vol. 48, no. 3, pp. 502–513, Mar. 2000.

[2] A. Abdi and M. Kaveh, "A space-time correlation model for multi-element antenna systems in mobile fading channels," *IEEE J. Select. Areas Commun.*, vol. 20, no. 3, pp. 550–560, Apr. 2002.

[3] M. Pätzold and B. O. Hogstad, "A space-time channel simulator for MIMO channels based on the geometrical one-ring scattering model," in *Proc. 60th IEEE Semiannual Veh. Technol. Conf., VTC 2004-Fall*. Sept. 2004, vol. 1, pp. 144–149, Los Angeles, CA, USA.

[4] A. Borhani and M. Pätzold, "A unified disk scattering model and its angle-of-departure and time-of-arrival statistics," *IEEE Trans. Veh. Technol.*, vol. 62, no. 2, pp. 473–485, Feb. 2013.

[5] K. T. Wong, Y. I. Wu, and M. Abdulla, "Landmobile radiowave multipaths' DOA-distribution: Assessing geometric models by the open literature's empirical datasets," *IEEE Trans. Antennas Propag.*, vol. 58, no. 2, pp. 946–958, Feb. 2010.

[6] A. Ispas, G. Ascheid, C. Schneider, and R. Thom, "Analysis of local quasi-stationarity regions in an urban macrocell scenario," in *Proc. 71th IEEE Vehicular Technology Conference, VTC 2010-Spring*. May 2010, Taipei, Taiwan.

[7] A. Gehring, M. Steinbauer, I. Gaspard, and M. Grigat, "Empirical channel stationarity in urban environments," in *Proc. 4th European Personal Mobile Communications Conference*. Feb. 2001, Vienna, Austria.

[8] D. Umansky and M. Pätzold, "Stationarity test for wireless communication channels," in *Proc. IEEE Global Communications Conference, IEEE GLOBECOM 2009*. Nov./Dec. 2009, Honolulu, Hawaii, USA.

[9] A. Paier, J. Karedal, N. Czink, H. Hofstetter, C. Dumard, T. Zemen, F. Tufvesson, A. F. Molisch, and C. F. Mecklenbräucker, "Characterization of vehicle-to-vehicle radio channels from measurement at 5.2 GHz," *Wireless Personal Communications (WPC)*, vol. 50, no. 1, pp. 19–32, July 2009.

[10] G. Matz, "On non-WSSUS wireless fading channels," *IEEE Trans. Wireless Commun.*, pp. 2465–2478, Sept. 2005.

[11] A. Ghazal, C. Wang, H. Hass, R. Mesleh, D. Yuan, and X. Ge, "A non-stationary MIMO channel model for high-speed train communication systems," in *Proc. 75th IEEE Vehicular Technology Conference, VTC 2012-Spring*. May 2012, Yokohama, Japan.

[12] A. Chelli and M. Pätzold, "A non-stationary MIMO vehicle-to-vehicle channel model based on the geometrical T-junction model," in *Proc. International Conference on Wireless Communications and Signal Processing, WCSP 2009*. Nov. 2009, Nanjing, China.

[13] J. Karedal, F. Tufvesson, N. Czink, A. Paier, C. Dumard, T. Zemen, C. F. Mecklenbräuker, and A. F. Molisch, "A geometry-based stochastic MIMO model for vehicle-to-vehicle communications," *IEEE Trans. Wireless Commun.*, vol. 8, no. 7, pp. 3646–3657, July 2009.

[14] A. Borhani and M. Pätzold, "A non-stationary one-ring scattering model," in *Proc. IEEE Wireless Commun. and Net. Conf. (WCNC'13)*. Apr. 2013, Shanghai, China.

[15] P. Pearle, B. Collett, K. Bart, D. Bilderback, D. Newman, and S. Samuels, "What Brown saw and you can too," *Am. J. Phys.*, vol. 78, no. 12, pp. 1278–1289, Dec. 2010.

[16] B. H. Fleury and D. Dahlhaus, "Investigations on the time variations of the wide-band radio channel for random receiver movements," in *Proc. IEEE International Symposium on Spread Spectrum Techniques and Applications (ISSSTA '94)*. vol. 2, pp. 631–636, Finland, Oulu.

[17] T. Camp, J. Boleng, and V. Davies, "A survey of mobility models for ad hoc network research," *Wireless Communications and Mobile Computing*, vol. 2, no. 5, pp. 483–502, Sept. 2002.

[18] A. Einstein, "Über die von der molekularkinetischen Theorie der Wärme geforderte Bewegung von in ruhenden Flüssigkeiten suspendierten Teilchen," *Annalen der Physik*, , no. 17, pp. 549–560, May 1905.

[19] P. Langevin, "Sur la théorie du mouvement brownien," *C. R. Acad. Sci. Paris*, , no. 146, pp. 530–533, 1908.

[20] D. S. Lemons and A. Gythiel, "On the theory of Brownian motion," *Am. J. Phys.*, vol. 65, no. 11, pp. 530–533, Nov. 1979.

[21] R. C. Earnshaw and E. M. Riley, *Brownian Motion: Theory, Modelling and Applications*, Nova Science Pub Inc, 2011.

[22] M. Pätzold, *Mobile Fading Channels*, Chichester: John Wiley & Sons, 2nd edition, 2011.

[23] W. C. Jakes, Ed., *Microwave Mobile Communications*, Piscataway, NJ: IEEE Press, 1994.

[24] A. Papoulis, *Probability, Random Variables, and Stochastic Processes*, New York: McGraw-Hill, 3rd edition, 1991.

[25] F. Hlawatsch and F. Auger, *Time-Frequency Analysis: Concepts and Methods*, London (UK): ISTE and Wiley, 2008.

[26] I. S. Gradshteyn and I. M. Ryzhik, *Table of Integrals, Series, and Products*, Elsevier Academic Press, 7th edition, 2007.

ISBN: 978-988-19253-1-2
ISSN: 2078-0958 (Print); ISSN: 2078-0966 (Online)